Inorganic Chemistry

Article

pubs.acs.org/IC

Electrocatalytic Reduction of Carbon Dioxide by Mn(CN)(2,2′-bipyridine)$(CO)_3$: CN Coordination Alters Mechanism

Charles W. Machan,[†,‡] Charles J. Stanton, III,[¶,‡] Jonathon E. Vandezande,[§] George F. Majetich,[¶] Henry F. Schaefer, III,[§] Clifford P. Kubiak,*[,†] and Jay Agarwal*[,§]

[†]Department of Chemistry and Biochemistry, University of California, San Diego, California 92093, United States

[¶]Department of Chemistry and [§]Center for Computational Quantum Chemistry, University of Georgia, Athens, Georgia 30602, United States

Supporting Information

ABSTRACT: MnBr(2,2′-bipyridine)$(CO)_3$ is an efficient and selective electrocatalyst for the conversion of CO_2 to CO. Herein, substitution of the axial bromide for a pseudohalogen (CN) is investigated, yielding Mn(CN)(2,2′-bipyridine)$(CO)_3$. This replacement shifts the first and second reductions to more negative potentials (−1.94 and −2.51 V vs Fc/Fc^+, respectively), but imparts quasi-reversibility at the first feature. The two-electron, two-proton reduction of CO_2 to CO and H_2O is observed at the potential of the first reduction. Data from IR spectroelectrochemistry, cyclic voltammetry, and controlled potential electrolysis indicate that this behavior arises from the disproportionation of two one-electron-reduced species to generate the catalytically active species. Computations using density functional theory are also presented in support of this new mechanism.

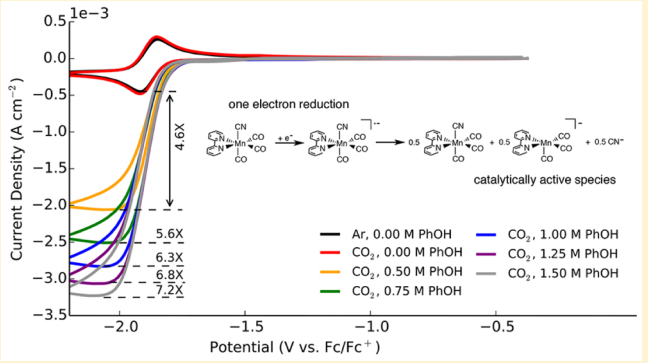

INTRODUCTION

In 2010, ∼33.5 × 10^9 t of carbon dioxide (CO_2) were emitted from fossil fuel combustion and cement manufacture globally,[1] up 8.8 × 10^9 t from the end of the previous decade. This elevated level of anthropogenic CO_2 emission continues to effect climate change,[2,3] underscoring the need for CO_2 recovery prior to atmospheric release and the development of utilization technology that harnesses CO_2 as a raw material.[4] To realize the latter objective, new processes must be identified for large-scale conversion that require minimal energy input along with cheap and abundant reagents. In this context, the electrocatalytic conversion of CO_2 to carbon monoxide (CO) using renewable energy and water is an intriguing solution.[5] Coupling this conversion with industrial Fischer−Tropsch chemistry could represent an efficient energy cycle that connects an abundant combustion byproduct to the generation of liquid fuels.

Prior research has established that a variety of materials are capable of binding and reducing CO_2 under an applied voltage, including metal electrodes,[6−12] surface-modified electrodes,[13−16] and homogeneous transition-metal catalysts.[5,17−24] This investigation is concerned with the latter: the use of soluble molecular electrocatalysts to shuttle redox equivalents from an electrode surface to CO_2 to effect selective reduction with minimal overpotential. Specifically, our interest is in manganese(I) tricarbonyl compounds, which have been shown to be effective mediators for the two-electron, two-proton reduction of CO_2 to CO in nonaqueous media with added Brønsted acids.[25−33] Notably, these species display high Faradaic efficiencies for CO—usually 85% to 100%—at relatively low overpotentials (∼500 mV).[25,26,28,33,34] (Compared to the standard potential, $E^0_{CO_2/CO,CH_3CN}$ = −0.650 V vs NHE, derived in ref 34.) In recent work, manganese(I) catalysts have also been utilized to mediate photochemical CO_2 reduction to formate.[35,36]

The most widely investigated manganese catalyst is MnBr(bpy)$(CO)_3$ where bpy = 2,2′-bipyridine. Some variation of the supporting bidentate ligand has been reported, including the extension of bpy with *tert*-butyl,[26] mesityl,[27] and phenol moieties.[31,37] Additionally, bpy has been replaced with an *N*-heterocyclic carbene (NHC)-pyridine framework[28,33] along with functionalized 1,4-diazobutadienes.[29,32] In any case, the proposed active species is a doubly reduced anion that possesses a vacant axial site for CO_2 coordination: $[Mn(\kappa^2\text{-L})(CO)_3]^-$ (**c**, see Scheme 1). Theoretical[38] and experimental[39,40] investigations of the mechanism suggest that one-electron reduction of the metal center causes the axial ligand, usually a bromide ion, to dissociate. Subsequently, the neutral radical monomer dimerizes to give $[Mn(\kappa^2\text{-L})(CO)_3]_2$ (**b**). The metal−metal bond within this species cleaves after loading

Received: July 30, 2015
Published: August 19, 2015

 © 2015 American Chemical Society

DOI: 10.1021/acs.inorgchem.5b01715
Inorg. Chem. 2015, 54, 8849−8856

Scheme 1. Summary of the Proposed Mechanism[38−40] for MnBr(κ^2-L) $(CO)_3$ Electrocatalysts, where κ^2-L is a Bidentate Ligand Such as 2,2′-Bipyridine

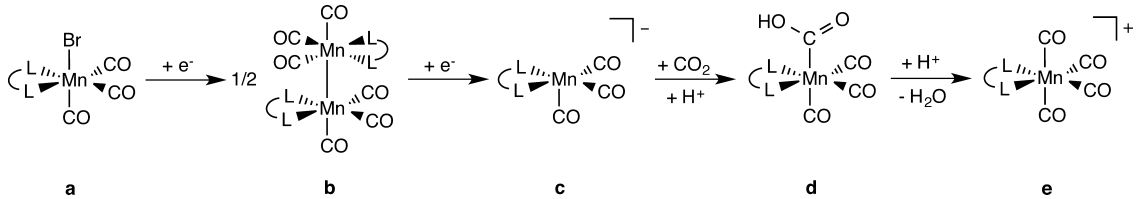

two additional electrons, yielding two monomers of the anionic, five-coordinate active species (**c**). Subsequent CO_2 coordination is rapid and irreversible. The resulting oxoanion is readily protonated, furnishing a Mn−COOH intermediate (**d**). The desired product (CO) is liberated from a proposed tetracarbonyl species, $[Mn(\kappa^2\text{-L})(CO)_4]^+$ (**e**), after carbon−oxygen bond cleavage within the hydroxycarbonyl moiety,[38] yielding a vacant site for the next cycle.

A requisite component of the catalytic process described is the availability of a coordination site to allow for CO_2 binding; bromide initially dissociates to yield the necessary vacancy, while liberation of the CO product in cycles thereafter allows for additional turnover. Bromide may also be substituted by other, labile ligands such as formate, and the same mechanism persists.[40] When bromine is replaced with a pseudohalogen such as NCS or CN, however, the Faradaic efficiency for CO production is diminished, concomitant with the formation of H_2 for NHC-pyridine based compounds.[33] The mechanism in this case is unclear: must the tricarbonyl core be retained for efficient catalysis, requiring dissociation of the pseudohalogen or may CO dissociate to provide a site for CO_2 coordination? Here, we explore the mechanism of CO_2 reduction using $Mn(CN)(bpy)(CO)_3$. Cyclic voltammetry, IR spectroelectrochemistry (IR-SEC), and computations are provided to support a disproportionation mechanism whereby the interaction of two one-electron-reduced complexes yields the catalytically active species: a two-electron-reduced complex lacking the axial CN ligand.

RESULTS AND DISCUSSION

Synthesis and Characterization. A genuine sample of $Mn(CN)(bpy)(CO)_3$ (**1**) was prepared via metathesis,[33] using $MnBr(bpy)(CO)_3$ and excess KCN. After workup, **1** was obtained in 93% yield and fully characterized using UV−vis, NMR, and FT-IR spectroscopies (see Supporting Information, Pages S1−S4). Crystals suitable for single-crystal X-ray analysis were obtained from the slow diffusion of pentanes into a solution of **1** dissolved in tetrahydrofuran (see Figure 1). The crystal structure confirms the expected octahedral geometry and *facial* arrangement of the tricarbonyl core.

Relative to the parent compound $MnBr(bpy)(CO)_3$, the UV−vis spectrum of **1** displays a blue-shifted metal-to-ligand charge transfer (MLCT) band (377 nm vs 416 nm[25]), which is aligned with the strong-field nature of CN^- compared to Br^-. Density functional theory (DFT) computations (see Theoretical Methods) predict a 5 kcal mol^{-1} increase in the highest occupied molecular orbital−lowest unoccupied molecular orbital gap energy as a result of cyanide substitution, which is consistent with the observed shift in MLCT band origin. The $^{13}C\{^1H\}$ NMR spectrum of **1** shows two resonances in the carbonyl region—one at 213 ppm and another at 221 ppm—indicating a vibrationally averaged C_s structure. These features

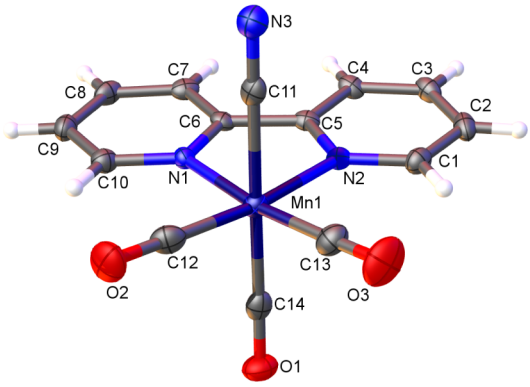

Figure 1. Molecular structure of $Mn(CN)(bpy)(CO)_3$ (**1**) obtained from X-ray diffraction (Z' = 2) with ellipsoids set at the 50% probability level. THF and H_2O molecules have been omitted for clarity.

are assigned to the sole axial carbonyl ligand and two equatorial carbonyl ligands, respectively. The carbon atom of cyanide resonates at 149 ppm.

Not surprisingly, the $^{13}C\{^1H\}$ NMR spectrum of $MnBr(bpy)(CO)_3$ closely matches that of **1**; corresponding resonances agree to within 1 ppm with the exception of a new peak for CN and a dramatic (8 ppm) upfield shift for the peak corresponding to C14 within the axial carbonyl (see Figure 1). Traditional bonding concepts fail to explain this disparity: an upfield shift generally indicates increased shielding from additional electron density around the nucleus, but substituting a π-donating ligand (Br; M ← L) for a π-accepting ligand (CN; M → L) should decrease back bonding to C14 as a result of a reduced charge on the Mn center. Indeed, natural bond orbital (NBO)[41] computations suggest diminished electron density on C14 as a result of substitution, including reduced occupation of the C14−O1 σ^* and π^* orbitals. Mayer bond analysis[42] also indicates an increased C14−O1 bond order. However, the computed $^{13}C\{^1H\}$ NMR chemical shifts for **1** correctly predict the upfield shift of C14 relative to the same atom in $MnBr(bpy)(CO)_3$. This suggests that another effect may be involved, such as shielding due to ring currents within the CN π orbitals,[43] but further investigation is required to develop an adequate understanding of the underlying electronic structure.

Cyclic Voltammetry. The cyclic voltammetry of **1** is presented in Figure 2. Scans were recorded under argon (Ar) in dry acetonitrile (MeCN) with 0.1 M tetrabutylammonium perchlorate (TBAP) supporting electrolyte at scan rates ranging from 10 to 2000 mV s^{-1}. Scanning to negative potentials at 100 mV s^{-1}, the first redox feature is observed at −1.94 V vs Fc/Fc^+ ($E_{1/2}$ = −1.91 V vs Fc/Fc^+). This is a one-electron, quasi-reversible process with peak-to-peak separation (ΔE_p) of 60 mV. At more negative potentials, a second, irreversible feature

DOI: 10.1021/acs.inorgchem.5b01715
Inorg. Chem. 2015, 54, 8849−8856

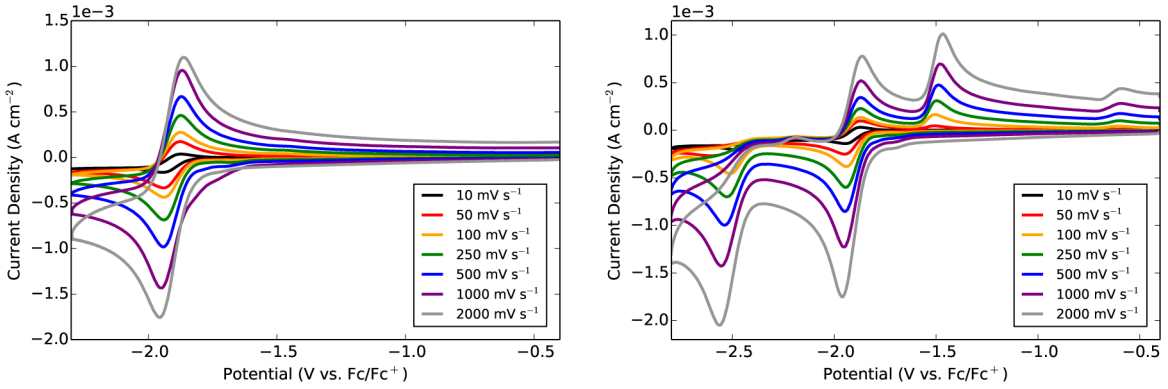

Figure 2. Cyclic voltammetry of $Mn(CN)(bpy)(CO)_3$ (**1**, 1 mM) under Ar in dry MeCN with 0.1 M TBAP supporting electrolyte. The switching potential was set to −2.2 V vs Fc/Fc^+ (left) or −2.8 V vs Fc/Fc^+ (right).

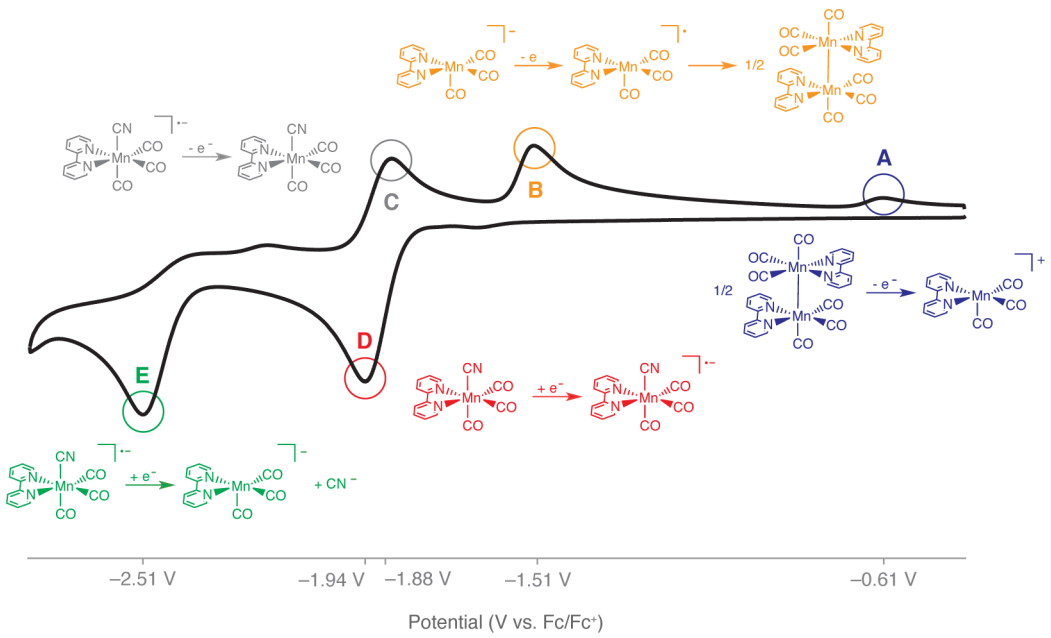

Figure 3. Cyclic voltammetry of $Mn(CN)(bpy)(CO)_3$ (**1**, 1 mM) under Ar in dry MeCN with 0.1 M TBAP supporting electrolyte at 100 mV s^{-1}. See text for descriptions of the redox features.

is observed at −2.51 V vs Fc/Fc^+. Both processes are diffusion-limited, as indicated by a linearly dependent relationship between the peak current and square root of the scan rate (see Page S11). The return scan from the second redox wave shows two new oxidative processes: one at −1.51 V vs Fc/Fc^+ and another at −0.61 V vs Fc/Fc^+. As shown in the left plot of Figure 2, these irreversible oxidations are absent if the switching potential is before the second reduction.

We ascribe the first reduction process at −1.94 V vs Fc/Fc^+ to a ligand-based reduction (see Figure 3, **D**); NBO computations indicate that 90% of the added charge resides on atoms within the bpy framework. Aligned with the reversibility observed in Figure 2, the optimized structure of $[Mn(CN)(bpy)(CO)_3]^{\bullet-}$ does not favor dissociation—the bond dissociation energies (BDE) for the axial CO and CN ligands are considerable at 31 and 23 kcal mol^{-1}, respectively. This stands in contrast to the behavior of $[MnBr(bpy)(CO)_3]^{\bullet-}$, which is observed to liberate Br^-.[38−40]

The second reduction wave at −2.51 V vs Fc/Fc^+ (**E**) is also ligand-based. Here, NBO computations suggest that 89% of the added charge is localized to bpy. In the optimized structure of $[Mn(CN)(bpy)(CO)_3]^{2-}$, the axial CO BDE remains significant (22 kcal mol^{-1}), but CN coordination is considerably weaker at 4 kcal mol^{-1}. Under experimental conditions, CN loss is nearly certain, which is supported by the observed irreversibility. Even increasing the scan rate to 2000 mV s^{-1} does not impart quasi-reversibility, indicating that the chemical change is very rapid on this time scale.

The oxidative processes at −0.61 V (**A**) and −1.51 V vs Fc/Fc^+ (**B**) may be assigned on the basis of previous literature reports. We designate process **A** as the oxidation of $[Mn(bpy)(CO)_3]_2$. Previously, the oxidation of several Mn−Mn dimers were observed in this region of the voltammogram: $[Mn(4,4'\text{-}tert\text{-butyl-bpy})(CO)_3]_2$ at −0.68 V vs Fc/Fc^+,[26] $[Mn(N\text{-methyl-}N'\text{-2-pyridylimidazol-2-ylidine})(CO)_3]_2$ at −0.63 V vs Fc/Fc^+,[33] and $[Mn(bpy)(CO)_3]_2$ at −0.60 V vs Fc/Fc^+.[25] (Values reported vs the saturated calomel electrode (SCE) and vs 10 mM Ag/Ag^+ were converted to vs Fc/Fc^+ by adding −0.380[44] and −0.087[45] V, respectively.) Presumably, axial CO loss in **1** could also yield the requisite vacancy for Mn−Mn bonding, but we eliminate this possibility on the grounds that (i) the computed BDE for the axial CO is roughly

DOI: 10.1021/acs.inorgchem.5b01715
Inorg. Chem. 2015, 54, 8849−8856

5 times that of CN, (ii) optimization of $[Mn(CN)(bpy)(CO)_2]_2^{2-}$ fails due to dissociation, and (iii) the addition of tetrabutylammonium cyanide (TBACN) to the electrolyte solution completely suppresses this feature (see Page S12).

The remaining feature at −1.51 V vs Fc/Fc^+ (**B**) is ascribed to the oxidation of $[Mn(bpy)(CO)_3]^-$. Bourrez et al. previously recorded the oxidation of $[Mn(bpy)(CO)_3]^-$ at −1.48 V vs Fc/Fc^+, which was assigned based on UV−vis spectroscopy.[25] Moreover, a similar wave appears in the CV of MnBr(4,4′-*tert*-butyl-bpy)$(CO)_3$ at ca. −1.6 V vs Fc/Fc^+ following two-electron reduction.[26] In these reports, where Br^- is available, the peak current for the oxidation of $[Mn(\kappa^2\text{-L})(CO)_3]^-$ is less than the peak current for oxidizing available Mn−Mn dimer. Here we observe the opposite pattern in peak current, suggesting that $[Mn(bpy)(CO)_3]^\bullet$ is captured by free CN^- before Mn−Mn bonding can occur, which is supported by the addition of TBACN as previously described. No evidence for an acetonitrile bound complex was observed (vide infra); in solution, CN^- is likely to outcompete MeCN for available coordination sites.

To gauge the ability for **1** to mediate CO_2 reduction, additional voltammograms were recorded under a CO_2 atmosphere in the presence of a Brønsted acid, either water (Figure 4) or phenol (Figure 5). With 5% added water, a slight

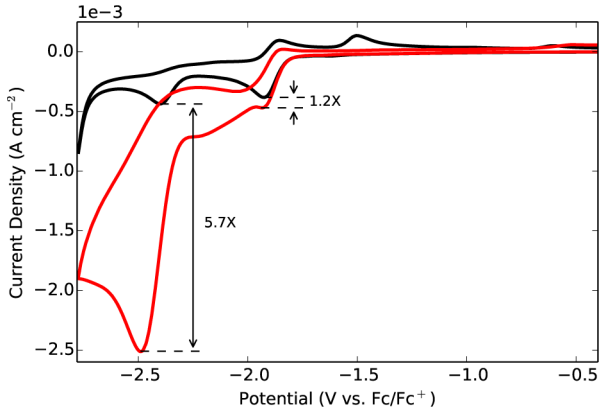

Figure 4. Cyclic voltammetry of $Mn(CN)(bpy)(CO)_3$ (**1**, 1 mM) under Ar (black) or CO_2 (red) in MeCN (5% H_2O) with 0.1 M TBAP supporting electrolyte at 100 mV s^{-1}. In the case of Ar, added water was pH adjusted to 3.7 to match the pH under CO_2.

current enhancement (1.2×) occurs at the peak current of the first reduction wave (ca. −1.94 V vs Fc/Fc^+) under CO_2 (red). At the potential of the second reduction (ca. −2.51 V vs Fc/Fc^+), a significant current enhancement (5.7×) is observed. We assign the majority of this enhancement to the catalytic reduction of CO_2 by a $[Mn(bpy)(CO)_3]^-$ active species, but caution that some reduction of water by glassy carbon is observed in control experiments at this very negative potential. The oxidation of $[Mn(bpy)(CO)_3]^-$ at ca. −1.51 V vs Fc/Fc^+ is absent from the return wave under CO_2, suggesting that this species is consumed.

When phenol is substituted for water as the Brønsted acid in solution (Figure 5), the voltammetry window shrinks (see Page S17 and ref 46), allowing only for the current enhancement at the first reduction to be probed. Note that in the absence of phenol no current enhancement is observed; the scan under CO_2 (red) matches that under Ar (black). As phenol is titrated into the electrolyte solution, current enhancement appears at the potential of the first reduction, from a 4.6× enhancement

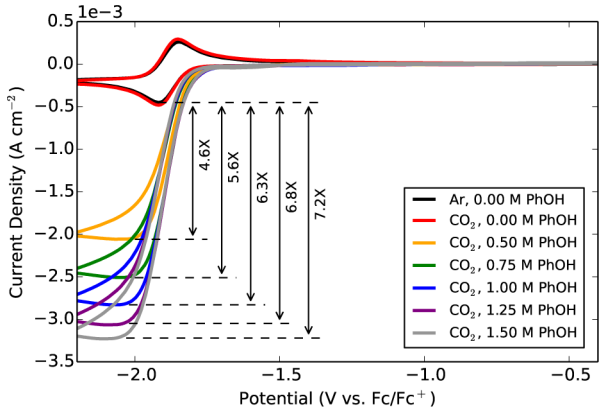

Figure 5. Cyclic voltammetry of $Mn(CN)(bpy)(CO)_3$ (**1**, 1 mM) under CO_2 in MeCN with added phenol (PhOH) and 0.1 M TBAP supporting electrolyte at 100 mV s^{-1}. A scan under Ar with no phenol (black) is shown for reference. Also see Page S16 for calculated turnover frequencies.

using 0.5 M phenol to a 7.2× enhancement using 1.5 M phenol. This superior activity when using phenol relative to water is aligned with previous reports of manganese catalysts.[38,47] Phenol is employed as a Brønsted acid in the remainder of this work.

Infrared Spectroelectrochemistry. IR-SEC allows for the direct interrogation of electrochemical reactions as a function of time and potential using IR spectroscopy.[39,48] In an effort to understand the behavior of **1** in the region of the first reduction—the lowest potential where catalytic current enhancement is observed—we recorded the IR spectrum at the resting potential and at the potential of the first reduction under an atmosphere of N_2 (Figure 6, left). At the resting potential (black), four IR bands are observed at 2115 (CN), 2029 (CO), 1942 (CO), and 1928 cm^{-1} (CO). The computed IR spectrum of **1**, scaled by 0.978 61 to account for the anharmonicity of the potential energy surface, qualitatively agrees with the observed transitions: the C−N stretch is predicted to appear at 2152 cm^{-1}, while the lone symmetric and two asymmetric stretches of the tricarbonyl group are predicted to appear at 2033, 1939, and 1930 cm^{-1}, respectively.

When the potential of the IR-SEC cell is stepwise shifted from resting to that of the first reduction (red; ca. −1.94 V vs Fc/Fc^+), five new bands appear at lower frequencies concomitant with the disappearance of the original spectrum. This red shift is expected: additional electron density should partially occupy the π^* orbitals of the CN and CO ligands, reducing their stretching frequencies. Curiously, the observed CO transitions (1911, 1837, and 1811 cm^{-1}) align best with the predicted frequencies for $[Mn(bpy)(CO)_3]^-$, a *two*-electron-reduced compound. The low-intensity band at 2007 cm^{-1} matches the computed symmetric CO stretch of $[Mn(CN)(bpy)(CO)_3]^{\bullet-}$ (2010 cm^{-1}), suggesting that the one-electron-reduced species is a minor product. The two remaining CO stretches for this compound (1909 and 1895 cm^{-1}) are predicted to have lower intensities than the symmetric stretch and would be concealed by the broad band at 1911 cm^{-1}. These data would suggest the possible disproportionation of two one-electron-reduced species, $[Mn(CN)(bpy)(CO)_3]^{\bullet-}$, formed at the potential of the first reduction.

To support this hypothesis we supplanted the applied voltage with a chemical reductant, $CoCp^*_2$, which possesses a redox potential of −1.91 V vs Fc/Fc^+.[44] Indeed, the same shift and

DOI: 10.1021/acs.inorgchem.5b01715
Inorg. Chem. 2015, 54, 8849−8856

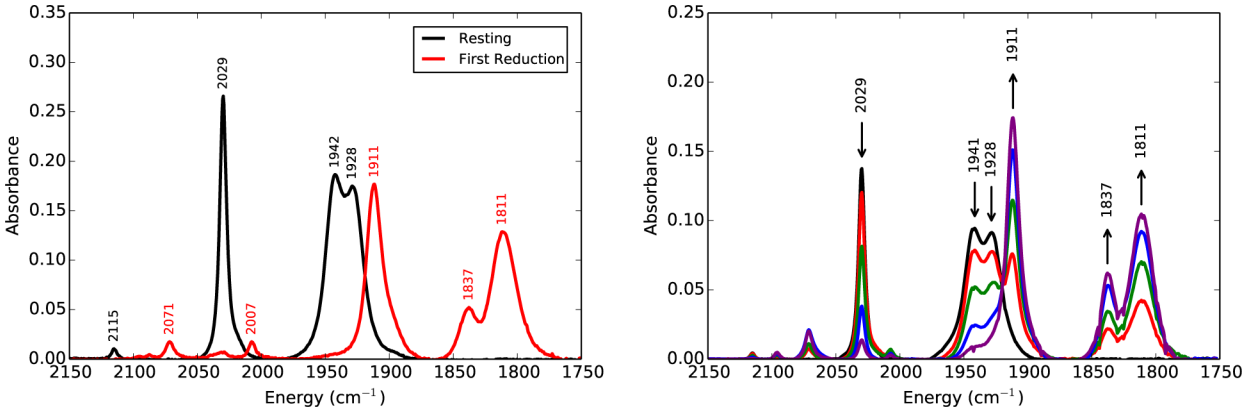

Figure 6. Infrared spectra of $Mn(CN)(bpy)(CO)_3$ (**1**) at controlled potentials (left) and with added chemical reductant (right) under an atmosphere of N_2. In the left plot, **1** (6.2 mM) was added to dry MeCN with 0.1 M $TBAPF_6$ supporting electrolyte. In the right plot, **1** (3 mM) was added to dry MeCN and titrated with $CoCp^*_2$ (black → purple; 0 → 2.1 equiv). Also see Page S15 for comparison with computational predictions.

Scheme 2. Proposed Disproportionation Mechanism Following One-Electron-Reduction, and Subsequent CO_2 Conversion to CO

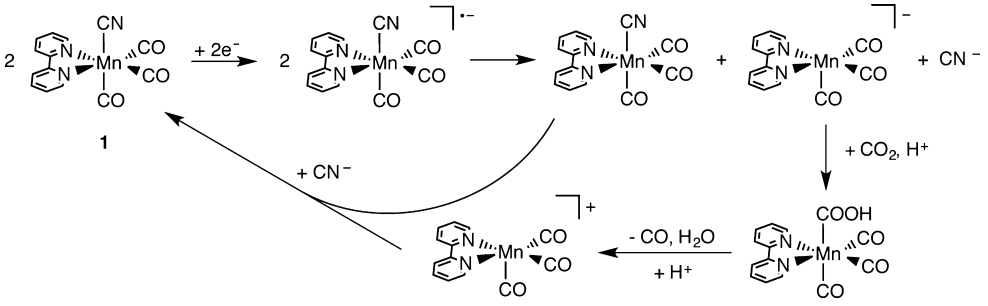

spectral pattern is observed as before (Figure 6, right). The intensities of the new bands in the CO stretching region (1911, 1837, and 1811 cm^{-1}) continue to rise after 1 equiv of $CoCp^*_2$ is added, supporting the formation of a two-electron product. Furthermore, the UV–vis spectrum of the product after adding 2.1 equiv of $CoCp^*_2$ shows new transitions at 352 and 559 nm (see Page S13), which agrees with previous assignments for $[Mn(bpy)(CO)_3]^-$.[25] The presence of an intermediary compound—such as $[Mn(bpy)(CO)_3]^•$, which could form from the slow dissociation of CN^- after one-electron reduction—is not observed. Spectra collected following the addition of substoichiometric equivalents of $CoCp^*_2$ (i.e., from 0 → 1 equiv) indicate only two compounds are present: the starting species $Mn(CN)(bpy)(CO)_3$ and the two-electon-reduced species $[Mn(bpy)(CO)_3]^-$.

In the cyclic voltammetry discussed above, Figure 2 shows no oxidative features for $[Mn(bpy)(CO)_3]^-$ (−1.51 V vs Fc/Fc^+) if the switching potential is before the second reduction, which is not aligned with a disproportionation mechanism unless the timescale is too short for appreciable formation of a two-electron species. To probe this, we electrolyzed **1** at the potential of the first reduction, then swept oxidatively to 0.0 V. After holding the voltage at −1.94 V vs Fc/Fc^+ for 120 s we observed a new peak consistent with the oxidation of $[Mn(bpy)(CO)_3]^-$ (see Page S14), consistent with a disproportionation reaction. From these data, we propose the mechanism shown in Scheme 2. Density functional theory computations predict the overall free energy (ΔG) of disproportionation to be −1 kcal mol^{-1}, though this near-equilibrium process should be driven by the loss of CN and the continuously applied potential. Under catalytic conditions, the thermodynamically favorable interaction of $[Mn(bpy)(CO)_3]^-$ with CO_2 in the presence of a Brønsted acid[38] should further accelerate disproportionation.

Controlled Potential Electrolysis. To understand the behavior of **1** under catalytic conditions, controlled potential electrolyses were performed both at the preparative scale in an IR-SEC cell and at the bulk scale with headspace analysis. To begin, the IR spectrum of **1** was recorded in MeCN with 0.1 M tetrabutylammonium hexafluorophosphate ($TBAPF_6$) and 0.5 M phenol in an IR-SEC cell. The expected transitions for the starting compound (**1**) were observed: [2119 (CN), 2031 (CO), 1943 (CO), and 1930 cm^{-1} (CO)], see Figure 7A. After sparging with CO_2 for 10 s, the potential of the IR-SEC cell was then set to the first reduction (ca. −1.9 V vs Fc/Fc^+), and sequential IR spectra were recorded roughly every minute for 5 min. Over time, the sharp bands assigned to phenol (1607 and 1596 cm^{-1}) decrease in intensity—note that all spectra were solvent-subtracted such that the depletion of PhOH is reflected as negative absorbance values—and two broad bands appear at 1654 and 1587 cm^{-1}. We assign the latter transition to phenoxide (PhO^-) from control experiments using NaOPh (see Page S18), while the band at 1654 cm^{-1} is assigned to water that is produced during the conversion of $CO_2 + 2H^+ + 2e^- \rightarrow CO + H_2O$. In the C–O stretching region only bands assigned to **1** are evident throughout the experiment, indicating that available $[Mn(bpy)(CO)_3]^-$ is rapidly consumed.

The potential of the IR-SEC cell was then increased to ca. −2.1 V vs Fc/Fc^+, and additional scans were recorded (Figure 7B). The continued consumption of phenol is evidenced by the decrease in intensity at 1607 and 1596 cm^{-1} along with an increase in intensity at 1587 cm^{-1}. Infrared transitions

DOI: 10.1021/acs.inorgchem.5b01715
Inorg. Chem. 2015, 54, 8849–8856

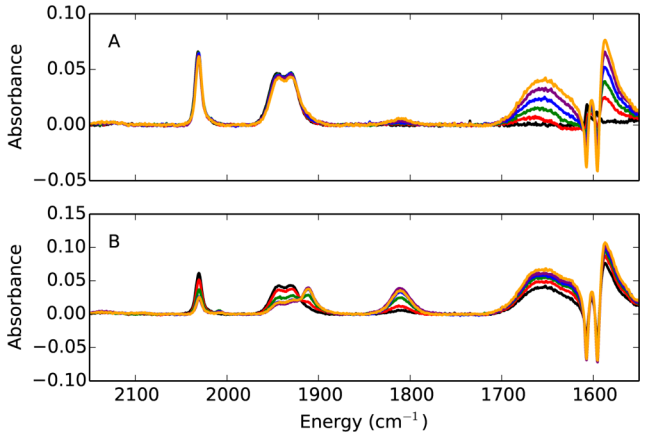

Figure 7. Infrared spectra of $Mn(CN)(bpy)(CO)_3$ (**1**, 7.9 mM) at ca. −1.9 V vs Fc/Fc^+ (A) then ca. −2.1 V vs Fc/Fc^+ (B) under an atmosphere of CO_2 in MeCN with 0.1 M $TBAPF_6$ supporting electrolyte and 0.5 M phenol. Scans were recorded roughly every minute (black → orange).

corresponding to the active species, $[Mn(bpy)(CO)_3]^-$, (1909 and 1805 cm^{-1}) begin to appear, since the rate of reduction of **1** should be faster at this potential and the available substrate diminishes over the time scale of the experiment.

Further analysis was performed at the bulk scale in a 70 mL custom reaction vessel with a graphite working electrode, platinum counter electrode, and Ag/AgCl pseudoreference electrode. These results are listed in Table 1. Across three trials

Table 1. Results from Three Controlled Potential Electrolyses at ca. −2.2 V vs Fc/Fc^+ with Analysis of the Headspace Using Gas Chromatography[a]

trial	charge passed	mol CO[b]	mol H_2[b]
1	3.40 C	1.70×10^{-4} (96%)	2.65×10^{-6} (2%)
2	3.20 C	1.60×10^{-4} (97%)	2.47×10^{-6} (1%)
3	3.40 C	1.79×10^{-4} (102%)	2.19×10^{-6} (1%)

[a]Compound **1** was loaded at a concentration of ∼0.9 mM in a 45 mL solution of MeCN with 0.1 M $TBAPF_6$ supporting electrolyte and 0.5 M phenol. [b]Faradaic efficiencies shown in parentheses.

at ca. −2.2 V vs Fc/Fc^+, analysis of the headspace with gas chromatography shows the presence of between 160 and 180 μmol of CO from ∼40 μmol of **1**, yielding an average Faradaic efficiency of 98% [average turnover number (TON) = 4]. Some H_2 is observed in each trial, but the average Faradaic efficiency is 1%, indicating excellent selectivity for CO_2 over available protons.

CONCLUSIONS

Literature reports of Mn(I) electrocatalysts have grown to encompass many derivatives of $MnBr(\kappa^2\text{-L})(CO)_3$, where κ^2-L can be functionalized or nonfunctionalized 2,2′-bipyridine, 1,4-diazobutadiene, or a pyridine-NHC construct. In this report, we have examined the replacement of Br for CN, yielding $Mn(CN)$(2,2′-bipyridine)$(CO)_3$. This substitution maintains the C_s symmetric, octahedral structure of the parent compound, but has a significant effect on the voltammetric response. Specifically, the first and second reduction potentials are shifted negative to −1.94 and −2.51 V vs Fc/Fc^+, respectively. The strong-field nature of CN imparts quasi-reversibility at the first feature, limiting the formation of $[Mn(bpy)(CO)_3]_2$. Indeed, the addition of tetrabutylammonium cyanide is found to completely surpress Mn−Mn bonding. At the second-reduction potential, CN dissociates to yield the catalytically active species $[Mn(bpy)(CO)_3]^-$.

From theoretical computations, chemical reductions, and IR SEC, we find that $[Mn(bpy)(CO)_3]^-$ may also be generated via the disproportionation of two one-electron-reduced compounds, allowing for the two-electron, two-proton reduction of CO_2 to CO and H_2O to nominally occur at the potential of the first reduction, −1.94 V vs Fc/Fc^+. Controlled potential electrolyses (three trials) performed at the potential of the first reduction (ca. −2.2 V vs Fc/Fc^+) with 0.5 M phenol yields average Faradaic efficiencies of FE_{CO} = 98% and FE_{H_2} = 1% over four turnovers, demonstrating the excellent selectivity of $Mn(CN)$(2,2′-bipyridine)$(CO)_3$ for reducing CO_2 over available protons, and further supporting the disproportionation mechanism. Future work will examine how the blue-shifted absorbance of this CN-substituted compound affects its lifetime under visible-light conditions.

EXPERIMENTAL METHODS

General. All reagents were obtained from commercial suppliers and used as received unless otherwise noted. Reactions were performed using standard Schlenk-line techniques under an atmosphere of argon. Methanol was dried prior to use by distilling it from CaH_2. ^1H NMR spectra were recorded on a Varian Mercury Plus 400 MHz spectrometer, and $^{13}C\{^1H\}$ NMR spectra were recorded on an Agilent DD2 600 MHz spectrometer. NMR chemical shifts were referenced to the residual protio signal of the deuterated solvent. Fourier transform infrared (FTIR) spectra were recorded on a ThermoNicolet 6700 spectrophotometer running OMNIC software. Absorption spectra were recorded on a CARY 300 Bio UV−vis spectrophotometer with a quartz cuvette (1 cm path length). $MnBr$(2,2′-bipyridine)$(CO)_3$ was prepared according to standard methods.[25]

Electrochemistry. Electrochemical experiments were performed using either a CH Instruments 601E or BAS Epsilon potentiostat. For all experiments, a single compartment cell was employed. A 3 mm diameter glassy carbon (GC) electrode (BASi or CH Instruments) was utilized as the working electrode (WE). The counter electrode (CE) was a platinum (Pt) wire, and the reference electrode (RE) was a silver/silver chloride (Ag/AgCl) electrode separated from solution by a Vycor or Teflon tip. Experiments were run with and without an added internal reference of ferrocene. Electrolyte solutions were composed of dry MeCN, containing 1 mM of catalyst and 0.1 M $TBAPF_6$ or 0.1 M TBAP supporting electrolyte, unless otherwise noted. The electrolyte was purged with Ar, N_2, or CO_2 before cyclic voltammograms were recorded and stirred between successive experiments. All voltammetry was referenced to an internal ferrocene standard, except for bulk electrolysis experiments where a pseudo-RE Ag/AgCl reference was employed.

Infrared Spectroelectrochemistry. The reader is referred to previous literature on IR-SEC from our laboratory for the cell design and setup.[39,48] A Pine Instrument Company model AFCBP1 bipotentiostat was employed for all measurements. During potential sweeps, thin layer bulk electrolysis was monitored by Fourier-transform reflectance IR off the electrode surface. All experiments were conducted in 0.1 M $TBAPF_6$/MeCN solutions and prepared with the catalyst under a nitrogen atmosphere. The IR-SEC cells include GC, Ag, and Pt electrodes for the WE, RE, and CE, respectively. As such, all potentials are referenced to a pseudo-RE, Ag/Ag^+ (silver wire; roughly +200 mV from the Fc/Fc^+ couple).

Controlled Potential Electrolysis. Trials were performed using a custom flask from Chemglass affixed with a custom PEEK lid with ports for three electrodes, purging, and sampling. A graphite WE, platinum CE, and Ag/AgCl pseudo-RE were employed. The system was sealed and tested for air-tightness before each run. In a typical trial, the flask was charged with a known amount of catalyst, 0.5 M phenol,

DOI: 10.1021/acs.inorgchem.5b01715
Inorg. Chem. 2015, 54, 8849−8856

stir bar, and electrolyte (0.1 M $TBAPF_6$ in MeCN) before being sparged to saturation with CO_2. To prevent the polymerization of PhOH on the counter electrode, 0.1 M Fc was added to the electrolyte solution as a sacrificial oxidant. After a completed run, the headspace was sampled via airtight syringe and characterized with gas chromatography. Each turnover for this system is based on two electron equivalents being passed for every catalyst molecule in solution.

Preparation of Mn(CN)(2,2′-Bipyridine)(CO)$_3$. MnBr(2,2′-Bipyridine)$(CO)_3$ (1.75 g, 4.7 mmol) and KCN (15.17g, 233.0 mmol) were suspended in 100 mL of MeOH and stirred at 60 °C under argon for 15 h. After it cooled to room temperature, the reaction mixture was diluted with H_2O (100 mL) and extracted with dichloromethane (3 × 100 mL). The combined organic extracts were washed with H_2O (100 mL) and brine (100 mL) and then dried over anhydrous $MgSO_4$ before filtration to remove the drying agent. Concentration under reduced pressure using a rotary evaporator gave the desired product as a light yellow solid (1.40 g, 93%). IR (ATR, cm^{-1}) ν_{CO}: 2022 (s), 1909 (s), 1887 (sh); ν_{CN}: 2108 (m). ^1H NMR (DMSO-d_6), 20 °C: δ 9.06 (2H, d, J = 4 Hz), 8.69 (2H, d, J = 8 Hz), 8.28−8.23 (2H, m), 7.75−7.72 (2H, m). $^{13}C\{^1H\}$ NMR (DMSO-d_6, 25 °C): δ 221.07, 213.13, 154.66, 153.28, 149.29, 139.14, 127.09, 123.42.

THEORETICAL METHODS

Computations were performed with DFT using the B3LYP functional[49−51] as implemented in Orca 3.0.1.[52] Optimized geometric parameters and harmonic vibrational frequencies were obtained with the inclusion of an implicit solvent model using the conductor like screening model (COSMO)[53] with the default values for acetonitrile (ϵ = 36.6). The def2-TZVP basis set[54] was used to describe all "light" atoms. Mn and Br were described with the LANL08(f)[55] and LANL2DZ[56,57] basis sets, respectively, and their corresponding effective core potentials. Vibrational analysis was used to confirm the nature of the stationary points as true minima. All structures were computed with tight convergence criteria (RMS force < 1×10^{-6} Hartree/bohr), and vibrational frequencies were scaled by 0.978 61 to account for the anharmonicity of the potential energy surface.

Natural bond orbital computations were performed with NBO5.[41] NMR computations were performed using the IGLO method[58,59] with the origin placed at the center of electronic charge and orbitals localized using Pipek−Mezey approach.[60] Previous studies indicate DFT-IGLO computations using this localization adequately describe the nuclei within ligands bound to transition metals.[61,62] Chemical shifts were first computed relative to DMSO, then converted relative to tetramethylsilane by adding 39.5 ppm.[63]

ASSOCIATED CONTENT

Supporting Information

The Supporting Information is available free of charge on the ACS Publications website at DOI: 10.1021/acs.inorgchem.5b01715.

NMR, FTIR, and UV-vis spectra, X-ray crystallography data, electrochemistry data, and stationary points from computations. (PDF)

X-ray crystallographic information of one compound. (CIF)

AUTHOR INFORMATION

Corresponding Authors

*E-mail: ckubiak@ucsd.edu. (C.P.K.)

*E-mail: jagarwal@uga.edu. (J.A.)

Author Contributions

‡C.W.M. and C.J.S. contributed equally to this work.

Notes

The authors declare no competing financial interest.

ACKNOWLEDGMENTS

Research at the Univ. of Georgia was supported by the National Science Foundation (NSF) under Grant No. CHE-1361178. G.F.M. acknowledges Donors of the American Chemical Society Petroleum Research Fund for partial support of this research (Grant No. 54228-ND1). We thank Dr. C. Moore for assistance in the acquisition and refinement of X-ray structures. C.W.M. and C.P.K. acknowledge support for this work from the AFOSR through a Basic Research Initiative (BRI) Grant (No. FA9550-12-1-0414).

REFERENCES

(1) Le Quéré, C.; et al. *Earth Syst. Sci. Data Discuss.* **2014**, *7*, 521−610.

(2) PALAEOSENS Project Members. *Nature* **2012**, *491*, 683−691.10.1038/491008b

(3) Song, C. *Catal. Today* **2006**, *115*, 2−32.

(4) Leitner, W. *Angew. Chem., Int. Ed. Engl.* **1995**, *34*, 2207−2221.

(5) Costentin, C.; Robert, M.; Savéant, J.-M. *Chem. Soc. Rev.* **2013**, *42*, 2423−2436.

(6) Medina-Ramos, J.; DiMeglio, J. L.; Rosenthal, J. *J. Am. Chem. Soc.* **2014**, *136*, 8361−8367.

(7) Hara, K.; Kudo, A.; Sakata, T. *J. Electroanal. Chem.* **1995**, *391*, 141−147.

(8) Chen, Y.; Li, C. W.; Kanan, M. W. *J. Am. Chem. Soc.* **2012**, *134*, 19969−19972.

(9) Gattrell, M.; Gupta, N.; Co, A. *J. Electroanal. Chem.* **2006**, *594*, 1−9.

(10) Kuhl, K. P.; Cave, E. R.; Abram, D. N.; Jaramillo, T. F. *Energy Environ. Sci.* **2012**, *5*, 7050−7059.

(11) Kuhl, K. P.; Hatsukade, T.; Cave, E. R.; Abram, D. N.; Kibsgaard, J.; Jaramillo, T. F. *J. Am. Chem. Soc.* **2014**, *136*, 14107−14113.

(12) Hori, Y. In *Modern Aspects of Electrochemistry;* Vayenas, C. G., White, R. E., Gamboa-Aldeco, M. E., Eds.; Springer: New York, 2008; Chapter 3, pp 89−189.

(13) Abruña, H. D. *Coord. Chem. Rev.* **1988**, *86*, 135−189.

(14) Ramos Sende, J. A.; Arana, C. R.; Hernández, L.; Potts, K. T.; Keshevarz-K, M.; Abruña, H. D. *Inorg. Chem.* **1995**, *34*, 3339−3348.

(15) O'Toole, T. R.; Margerum, L. D.; Westmoreland, T. D.; Vining, W. J.; Murray, R. W.; Meyer, T. J. *J. Chem. Soc., Chem. Commun.* **1985**, 1416−1417.

(16) Christensen, P.; Hamnett, A.; Muir, A. V. G.; Timney, J. A.; Higgins, S. *J. Chem. Soc., Faraday Trans.* **1994**, *90*, 459−469.

(17) Grice, K. A.; Kubiak, C. P. *Adv. Inorg. Chem.* **2014**, *66*, 163−188.

(18) Schneider, J.; Jia, H.; Muckerman, J. T.; Fujita, E. *Chem. Soc. Rev.* **2012**, *41*, 2036−2051.

(19) Collin, J. P.; Sauvage, J. P. *Coord. Chem. Rev.* **1989**, *93*, 245−268.

(20) Sullivan, B. P.; Bolinger, C. M.; Conrad, D.; Vining, W. J.; Meyer, T. J. *J. Chem. Soc., Chem. Commun.* **1985**, 1414−1415.

(21) Keene, F. R.; Sullivan, B. P. *Electrochemical and Electrocatalytic Reactions of Carbon Dioxide;* Sullivan, B. P., Krist, K., Guard, H. E., Eds.; Elsevier: Amsterdam, 1993.

(22) Bruce, M. R. M.; Megehee, E.; Sullivan, B. P.; Thorp, H. H.; O'Toole, T. R.; Downard, A.; Pugh, J. R.; Meyer, T. J. *Inorg. Chem.* **1992**, *31*, 4864−4873.

(23) Ishida, H.; Tanaka, K.; Tanaka, T. *Organometallics* **1987**, *6*, 181−186.

(24) Clark, M. L.; Grice, K. A.; Moore, C. E.; Rheingold, A. L.; Kubiak, C. *Chem. Sci.* **2014**, *5*, 1894−1900.

(25) Bourrez, M.; Molton, F.; Chardon-Noblat, S.; Deronzier, A. *Angew. Chem., Int. Ed.* **2011**, *50*, 9903−9906.

DOI: 10.1021/acs.inorgchem.5b01715
Inorg. Chem. 2015, 54, 8849−8856

(26) Smieja, J. M.; Sampson, M. D.; Grice, K. A.; Benson, E. E.; Froehlich, J. D.; Kubiak, C. P. *Inorg. Chem.* **2013**, *52*, 2484−2491.
(27) Sampson, M. D.; Nguyen, A. D.; Grice, K. A.; Moore, C. E.; Rheingold, A. L.; Kubiak, C. P. *J. Am. Chem. Soc.* **2014**, *136*, 5460−5471.
(28) Agarwal, J.; Shaw, T. W.; Stanton, C. J.; Majetich, G. F.; Bocarsly, A. B.; Schaefer, H. F. *Angew. Chem., Int. Ed.* **2014**, *53*, 5152−5155.
(29) Zeng, Q.; Tory, J.; Hartl, F. *Organometallics* **2014**, *33*, 5002−5008.
(30) Walsh, J. J.; Neri, G.; Smith, C. L.; Cowan, A. J. *Chem. Commun.* **2014**, *50*, 12698−12701.
(31) Franco, F.; Cometto, C.; Ferrero Vallana, F.; Sordello, F.; Priola, E.; Minero, C.; Nervi, C.; Gobetto, R. *Chem. Commun.* **2014**, *50*, 14670−14673.
(32) Vollmer, M. V.; Machan, C. W.; Clark, M. L.; Antholine, W. E.; Agarwal, J.; Schaefer, H. F., III; Kubiak, C. P.; Walensky, J. R. *Organometallics* **2015**, *34*, 3−12.
(33) Agarwal, J.; Stanton, C. J., III; Vandezande, J. E.; Majetich, G. F.; Bocarsly, A. B.; Schaefer, H. F., III; Shaw, T. W. *Dalton Trans.* **2015**, *44*, 2122−2131.
(34) Costentin, C.; Drouet, S.; Robert, M.; Savéant, J.-M. *Science* **2012**, *338*, 90−94.
(35) Takeda, H.; Koizumi, H.; Okamoto, K.; Ishitani, O. *Chem. Commun.* **2014**, *50*, 1491−1493.
(36) Fei, H.; Sampson, M. D.; Lee, Y.; Kubiak, C. P.; Cohen, S. M. *Inorg. Chem.* **2015**, *54*, 6821−6828.
(37) Agarwal, J.; Shaw, T. W.; Schaefer, H. F.; Bocarsly, A. B. *Inorg. Chem.* **2015**, *54*, 5285−5294.
(38) Riplinger, C.; Sampson, M. D.; Ritzmann, A. M.; Kubiak, C. P.; Carter, E. A. *J. Am. Chem. Soc.* **2014**, *136*, 16285−16298.
(39) Machan, C. W.; Sampson, M. D.; Chabolla, S. A.; Dang, T.; Kubiak, C. P. *Organometallics* **2014**, *33*, 4550−4559.
(40) Grills, D. C.; Farrington, J. A.; Layne, B. H.; Lymar, S. V.; Mello, B. A.; Preses, J. M.; Wishart, J. F. *J. Am. Chem. Soc.* **2014**, *136*, 5563−5566.
(41) Glendening, E. D.; Badenhoop, J. K.; Reed, A. E.; Carpenter, J. E.; Bohmann, J. A.; Morales, C. M.; Weinhold, F. *NBO 5.0;* University Of Wisconsin, Madison: Madison, WI, 2001.
(42) Mayer, I. *Int. J. Quantum Chem.* **1984**, *26*, 151−154.
(43) Friebolin, H. *Basic One- and Two-Dimensional NMR Spectroscopy;* Wiley-VCH Verlag GmbH & Co. KGaA: Weinheim, Germany, 2011.
(44) Connelly, N. G.; Geiger, W. E. *Chem. Rev.* **1996**, *96*, 877−910.
(45) Pavlishchuk, V. V.; Addison, A. W. *Inorg. Chim. Acta* **2000**, *298*, 97−102.
(46) McCarthy, B. D.; Martin, D. J.; Rountree, E. S.; Ullman, A. C.; Dempsey, J. L. *Inorg. Chem.* **2014**, *53*, 8350−8361.
(47) Riplinger, C.; Carter, E. A. *ACS Catal.* **2015**, *5*, 900−908.
(48) Zavarine, I. G.; Kubiak, C. P. *J. Electroanal. Chem.* **2001**, *495*, 106−109.
(49) Becke, A. D. *J. Chem. Phys.* **1993**, *98*, 5648−5652.
(50) Becke, A. D. *J. Chem. Phys.* **1996**, *104*, 1040−1046.
(51) Lee, C. T.; Yang, W. T.; Parr, R. G. *Phys. Rev. B: Condens. Matter Mater. Phys.* **1988**, *37*, 785−789.
(52) Neese, F. *WIREs Comput. Mol. Sci.* **2012**, *2*, 73−78.
(53) Klamt, A.; Shuurmann, G. *J. Chem. Soc., Perkin Trans. 2* **1993**, *5*, 799−805.
(54) Weigend, F.; Ahlrichs, R. *Phys. Chem. Chem. Phys.* **2005**, *7*, 3297−3305.
(55) Roy, L. E.; Hay, P. J.; Martin, R. L. *J. Chem. Theory Comput.* **2008**, *4*, 1029−1031.
(56) Ehlers, A. W.; Böhme, M.; Dapprich, S.; Gobbi, A.; Höllwarth, A.; Jonas, V.; Köhler, K. F.; Stegmann, R.; Veldkamp, A.; Frenking, G. *Chem. Phys. Lett.* **1993**, *208*, 111−114.
(57) Hay, P. J.; Wadt, W. R. *J. Chem. Phys.* **1985**, *82*, 270.
(58) Kutzelnigg, W. *Isr. J. Chem.* **1980**, *19*, 193−200.
(59) Schindler, M.; Kutzelnigg, W. *J. Chem. Phys.* **1982**, *76*, 1919−1933.
(60) Pipek, J.; Mezey, P. G. *J. Chem. Phys.* **1989**, *90*, 4916−4926.
(61) Kaupp, M. *Chem. - Eur. J.* **1996**, *2*, 348−358.
(62) Kaupp, M.; Malkina, O. L.; Malkin, V. G. *J. Chem. Phys.* **1997**, *106*, 9201−9212.
(63) Gottlieb, H. E.; Kotlyar, V.; Nudelman, A. *J. Org. Chem.* **1997**, *62*, 7512−7515.

DOI: 10.1021/acs.inorgchem.5b01715
Inorg. Chem. 2015, 54, 8849−8856